Effect of Hydrocarbon Resin on the Morphology and Mechanical Properties of Isotactic Polypropylene/Clay Composites

Sossio Cimmino, Clara Silvestre, Donatella Duraccio, Marilena Pezzuto

Istituto di Chimica e Tecnologia dei Polimeri (ICTP), CNR, Pozzuoli 80078, NA, Italy

Received 2 February 2010; accepted 26 April 2010
DOI 10.1002/app.32745
Published online 30 July 2010 in Wiley Online Library (wileyonlinelibrary.com).

ABSTRACT: The article reports an investigation of the effect of a hydrocarbon resin, Necirés TR100, on the structure, morphology, and properties of two isotactic polypropylene/clay composites. The clays are Dellite HPS, a purified montmorillonite, and Dellite 67G, a purified and modified montmorillonite with a high content of quaternary ammonium salt. Necirés TR100 contains hydroxyl and acid groups, which were expected to interact during the melt mixing with the polar surface of the clays to have intercalation with Dellite HPS and/or exfoliation of Dellite 67G, which is already intercalated by the quaternary ammonium salt. The morphological results indicate that the composite isotactic polypropylene/Dellite HPS presents large and coarse clay domains, whereas the composite isotactic polypropylene/Dellite 67G presents a better distribution of the clay clusters, although the presence of some clay domains of a few μm are also detected. Although results from Wide Angle X-ray Diffraction have indicated that Necirés TR100 has no effect on the layers distance of Dellite HPS and Dellite 67G its addition produces composites with clay particles homogenously distributed in the polyolefin matrix, better tensile properties (higher values of Young's modululs and elongation to break) and decrease of permeability. © 2010 Wiley Periodicals, Inc. J Appl Polym Sci 119: 1135–1143, 2011

Key words: composites; clay; mechanical properties; morphology

INTRODUCTION

One of the most promising nanocomposite systems is based on polymers and clay minerals consisting of layered silicates.[1–31] These systems have attracted great interest, both in industry and in academia, because they often exhibit remarkable improvement of properties when compared with those of pure polymer or conventional composites. These improvements include: mechanical properties,[2,14,21,26,28,30,31] heat resistance,[11,25] barrier properties,[1,3,8,15,29] and flammability[12,25]; increased biodegradability in the case of biodegradable polymers.[17,18] Of course not all the polymers are equally well-suited for polymer-layered silicate nanocomposite development. The exfoliated and homogeneous dispersion of the silicate layers can be achieved only in the case of polymers containing polar-functional groups, i.e. amide[7] and imide groups.[2] This is mostly due to the fact that the silicate layers of the clay have polar hydroxyl groups and are compatible only with polymers containing polar functional groups.

Isotactic polypropylene (iPP) is a semicrystalline thermoplastic polymer with a large range of applications[32,33] because of its attractive combination of good processability, mechanical properties, and chemical resistance. To increase the use of iPP in the fields where this polymer presents some limitations (due for example to high flammability, low stiffness at high temperature, and not elevated barrier properties), numerous studies on iPP modified by adding smectite clays have been carried out especially lately by using maleic anhydride grafted polypropylene.[21–28]

Usuki et al.[34] reported a different approach to prepare an iPP/clay hybrid by using a functional oligomer. To obtain complete or sufficient dispersion of the silicate layers in the polymer matrix the structure of the oligomer has to be considered: the oligomer molecule must have a certain amount of polar groups necessary for the intercalation between silicate layers by hydrogen bond formation; the oligomer should be compatible with iPP. Preliminary work[35] has shown that the resin Necirés TR100 is compatible with iPP up to 30% in weight (upper limit investigated) and it results just suitable for this investigation because it contains hydroxyl and acid groups.

Correspondence to: S. Cimmino (cimmino@icp.cnr.it).
Contract grant sponsor: European Community's Seventh Framework Programme; contract grant number: 218331 NaPolyNet.

© 2010 Wiley Periodicals, Inc.

In this work, the aim is to investigate the effect of the Necirés TR100 on the properties (as stress and elongation to break, Young's modulus and permeability to water vapor) of two iPP composites, one containing Dellite HPS (a purified montmorillonite), and the second composite containing Dellite G67 (a purified montmorillonite modified with a high content of quaternary ammonium salt). Dellite 67G is chosen to investigate if any interaction is possible between the hydroxyl and acid groups of the resin Necirés TR100 and those of the ammonium quaternary salt.

EXPERIMENTAL

Materials

The isotactic polypropylene (iPP) is a commercial product, Moplen S30S (kindly provided by Basell, Ferrara, Italy) with a melt flow index of 1.8 g/10 min. The clays used are Dellite HPS and Dellite 67G, kindly supplied by Laviosa Chimica Mineraria SpA, Italy. Dellite HPS and Dellite 67G are derived from a naturally occurring especially purified montmorillonite; the difference is that Dellite 67G is then modified with a high content of quaternary ammonium salt (dimethyl dehydrogenated tallow ammonium). Dellite 67G and Dellite HPS are reported by the producing company to be both particularly useful additives to improve various physical and thermo-mechanical properties of various polymers, as polyolefins, polyester, polystyrene, etc. The expected advantages in polymer systems are on barrier, thermal stability, stiffness, solvent/chemical resistance, weight reduction, flame retardant, and antidropping. From now through the paper they will be reported as HPS and 67G, respectively.

The hydrocarbon resin, used to investigate the possibility to improve compatibility between iPP and clays, is Necirès TR100 provided by Neville Chemical Europe BV (The Netherlands). Necirès TR100 is a thermoplastic hydrocarbon resin based on cycloaliphatic monomers with hydroxyl value 40 and acid value 7 and from now, it is reported for simplicity only as TR100. It is chosen to use a fixed quantity of TR100, 10% in weight of the blend iPP + TR100, which is generally the average percentage used by the packaging industries. The amount of clay added to the blend was fixed to be 3 g for every 100 g of iPP + TR100. The clay producing company indicates two methods to incorporate the clay in thermoset and thermoplastic systems; (i) adding directly the clay to the compound; (ii) adding up to 50% of clay in a master batch and then diluting the material in the final compound. In this work, it was used the first method, that is, the direct addition of the clay to the compound because the blends were prepared in a mixing chamber of a Brabender-like apparatus. The second method is more indicated when the mixtures are prepared by using an extruder. The compositions of the systems are given in Table I.

TABLE I
Composite System Composition

Formulation code	iPP (wt %)	TR100 (wt %)	Dellite HPS	Dellite 67G
iPP	100	–	–	–
iPP/TR100	90	10	–	–
iPP/HPS	97	–	3 wt %	–
iPP/TR100/HPS	90	10	3 pph[a]	–
iPP/67G	97	–	–	3 wt %
iPP/TR100/67G	90	10	–	3 pph[a]

[a] Part (or grams) per hundred parts (or grams) of iPP + TR100.

The hybrid systems were prepared by melt mixing in a Brabender-like apparatus at 210°C and 32 rpm; the mixing time was 10 min. Slabs and films were prepared by compression molding in a press at 210°C for 3 min without applied pressure to allow complete melting and for other 3 min with the pressure raised to 2×10^{10} Pa. Then the plates of the press, fitted with cooling coils, were rapidly cooled to room temperature by using cold water. Finally the pressure was released and the mold, with a rectangular shape $1 \times 70 \times 110$ mm, removed from the press. Films with thickness of 80 μm were obtained by using the same procedure utilized for the compression-molded samples but with a pressure at 15,000 pounds.

WAXD analysis

Wide Angle X-ray Diffraction was carried out by using a Philips diffractometer (PW 1050) operating at the CuK_α radiation. Measurements of diffracted intensity were made in the angular range of 3–45° (2θ), at room temperature. The crystalline percentage was calculated with the following procedure. The baseline was drawn between two points [Fig. 1(A)], which were chosen so that all diffraction patterns has minima at these points; the amorphous area (A_a) was chosen by a line being drawn that connected the two extreme minimum points of the baseline and the minimums of the crystalline peaks. The crystalline percentage (X_c) for plain iPP and for the blend and composites (in the second column of Table II) was calculated as ratio of the area under the crystalline peaks (A_c) to the total area ($A_c + A_a$), multiplied by 100:

$$X_c = \frac{A_c}{A_c + A_a} \times 100 \quad (1)$$

The crystalline percentage referred to only iPP in the case of blend/composite containing 10% in wt of

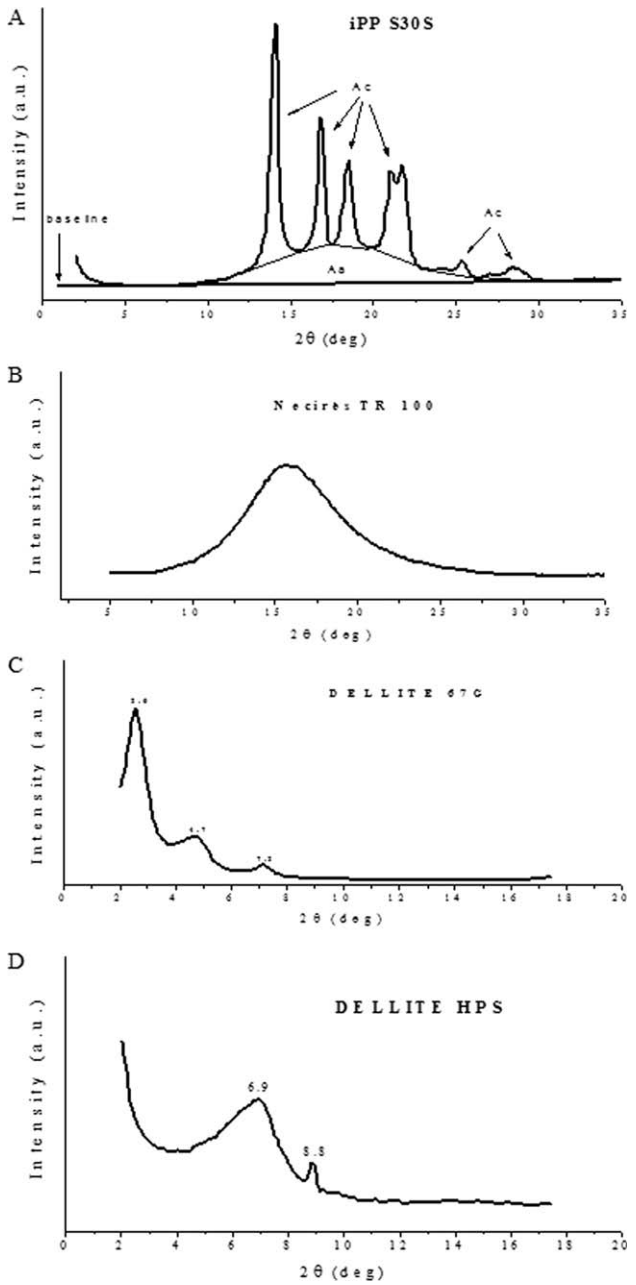

Figure 1 WAXD profiles of iPP (A), TR100 (B), Dellite 67G (C), and Dellite HPS (D).

Necires TR100 (reported in the third column of Table II), is given by the ratio, multiplied by 100, of the area under crystalline peaks (A_c) to the sum of the area under the crystalline peaks (A_c) and the area of the amorphous peaks multiplied by the iPP percentage in the blend (0.9):

$$X_c = \frac{A_c}{A_c + 0.9A_a} \times 100 \quad (2)$$

SEM analysis

SEM analysis was performed with a Philips 501 SEM (Philips, The Netherlands) after vacuum metallization of the samples by means of a Polaron sputtering apparatus with Au-Pd alloy. Samples for SEM analyses were prepared by fracturing in liquid nitrogen the compression molding samples.

Thermal analysis

The calorimetric properties of the compression-molded blends were investigated with a differential scanning calorimeter (Mettler DSC822). The apparatus was calibrated with pure indium at various scanning rates. About 10 mg of the sample was fast heated from room temperature to 200°C, kept at this temperature for 2 min and then cooled to −80°C at rate of 50°C/min; finally the thermo-analytical curve was recorded during the heating from −80 to 200°C at a rate of 20°C/min. The melting temperature (T_m) was obtained from the maxima of the endothermic peaks and the glass transition temperature (T_g) at the maximum of the peak obtained by applying the first derivative procedure.

Thermogravimetric

The thermal stability of samples was conducted using a TGA/SDTA 851 Mettler instrument at a scan rate of 20°C/min from 25 to 700°C in air atmosphere.

Tensile mechanical test

Dumb-bell-shaped specimens (Type IV according to ASTM D638) were cut from the slab using a steel punch cutter. Stress–strain curves were obtained by using an Instron machine (Model 4505) at room temperature (ca. 21–25°C) at a crosshead speed of 5 mm/min. Young's modulus, stress and strain at yield and at break points were calculated from such curves on an average of 12 specimens.

Water vapor permeability

Water vapor permeability test was conducted according to ASTM E96 for the water method. The instrumental apparatus is a Multiperm Extra

TABLE II
Crystallization Index from Wide Angle X-Ray Diffractograms of Composites [X_c (composites)] and Values Normalized to iPP in the Blend [X_c (iPP)]

Composites	X_c (composite) (±2%)	X_c (iPP) (±2%)
iPP	55	55
iPP/TR100	50	55
iPP/HPS	54	54
iPP/TR100/HPS	50	55
iPP/67G	53	53
iPP/TR100/67G	51	56

Solution. It consists of a double chamber diffusion cell. The film is inserted between the two chambers: a nitrogen flux with water vapor enters in the lower one and a nitrogen flux enters in the upper one. The water vapor diffusion though the film is measured by a zirconium oxide sensor. The area of the film involved in the experiment is 1.76 cm^2. Measurements were carried out by using "tropical conditions" that are 90% of U.R. and 38°C. Collected data are converted in water vapor transmission rate (WVTR) that is defined as the steady vapor flow in time through an area of a body, normal to specific conditions of temperature and humidity at each surface. The results are reported in water vapor permeability that is the time rate of water vapor transmission through the area of a flat material of a certain thickness induced by a vapor pressure difference between two specific surfaces. Three experiments for each sample composition were performed.

RESULTS AND DISCUSSION

Figure 1 reports the WAXD profiles of compression molded iPP, and the profiles of TR100, 67G and HPS as received by the companies. It is recalled that iPP can present several crystalline forms, as α, β, γ and a mesomorphic form.[36,37] The presence of the α-form is revealed by the peak between 2θ = 18–19° in the diffraction pattern, corresponding to the (130) plane, β-form is detectable by the peak at 15.5–16.5°, corresponding to the (200) β plane whereas γ-form is detectable by the peak at 20° corresponding to the (117) plane. The α form is that generally present in iPP obtained from cooling or quenching from the melt. The γ phase is obtainable for high MW by crystallization at elevated pressure. Figure 1(A) shows that the iPP in the compression molded sample crystallizes prevalently in the monoclinic α-form. Figure 1(B) shows the diffractogram of TR100. The spectrum has the typical shape of an amorphous material. The WAXD profile of 67G, Figure 1(C), presents three peaks at 2.6° (d = 33.9A), 4.7° (d = 18.8A), and 7.2° (d = 12.3A), indicating a multilayer structure. The peak at 7.2° is generated by the pristine MMT interlayer distance, whereas the two peaks at 2.6 and 4.7° indicate a bimodal modification due to the expansion of interlayer distance generated by the intercalation between the layers of dimethyl dehydrogenated tallow ammonium. The WAXD profile of HPS, Figure 1(D), shows a peak at 6.9° (d = 12.8A) and a spike at 8.8° indicating a uniform layer structure.

Figure 2 reports the spectrum of the iPP/TR100 blend, and the spectra of the binary and ternary composites. The WAXD spectrum of iPP/TR100 shows that iPP contains besides crystals in α form also a small quantity of β crystals as it is deducible from the shoulder at 15.5–16.5° [Fig. 2(A)], indicating that TR100 resin acts as nuclei agent for the formation of β form crystals.

The WAXD profiles of the binary [(Fig. 2(B,D)] and ternary composites [Figs. 2(C,E)] show, besides the predominant α crystals and small quantity of β crystals, also the presence of γ crystals, as revealed by the peak at 20°. It seems possible to conclude that the γ form is formed only in samples containing HPS and 67G clays; in fact no peak or shoulder is detectable on the spectra of iPP and iPP/TR100.

The analysis of the diffraction patterns of the blends containing clays at low 2θ values (between 2 and 10°) can give information about the possible occurrence of intercalation and exfoliation. On the spectra of iPP/HPS [Fig. 2(B)] and iPP/TR100/HPS [Fig. 2(C)] it is well evident the reflection at 2θ = 6.9°, which is the same value of the plain HPS, as it is shown in Figure 1(C); the TR100 does not induce any intercalation of HPS. Passing to the analysis of iPP/67G spectrum, two well defined peaks at 2θ = 3.5 and 6.9° are found, whereas the plain 67G clay present three peaks at 2θ = 2.6, 4.7, and 7.2° [Fig. 1(D)]. The spectrum of the iPP/TR100/67G, in Figure 2(E), presents again the three peaks (at 2.4, 4.7, and 7.0°).

The peak at 3.5° in Figure 2(D) for iPP/67G could be probably due to the merging of the two peaks of clay at 2.6° and 4.7°, but at moment there is no explanation why they are merged in the binary composite and instead separated in the ternary composites [Fig. 2(E)]. The expectation that TR100 could have increased the intercalation of the clay or even induced exfoliation of the clay is clearly demonstrated not occurring by the spectrum in Figure 2(E).

Table II reports the crystallinity values of the blends and the values normalized to the iPP content. The crystallinity values normalized to the iPP content in the composites result constant with the composition (55 ± 2%), indicating that during the cooling from the melt the TR100 resin and the two clays do not have any significant influence on the crystallization degree of iPP.

Micrographs of fractured surfaces of compression molded samples, performed by SEM, are shown in Figure 3. Figure 3(A,B) are reported as comparison micrographs; it is worth to note that TR100 is completely compatible with iPP, in fact no domain or separated phase is observable in Figure 3(B) at least for the magnification used. The fractured surface of iPP/HPS [Fig. 3(C)] shows many domains of HPS, coarsely distributed in iPP matrix. The fractured surfaces of iPP/67G [Fig. 3(E)] shows instead less and smaller domains of the clay. This different degree of homogenization of the clay in iPP could be due to the different nature of the two clays: HPS is simply a purified montmorillonite; 67G is a

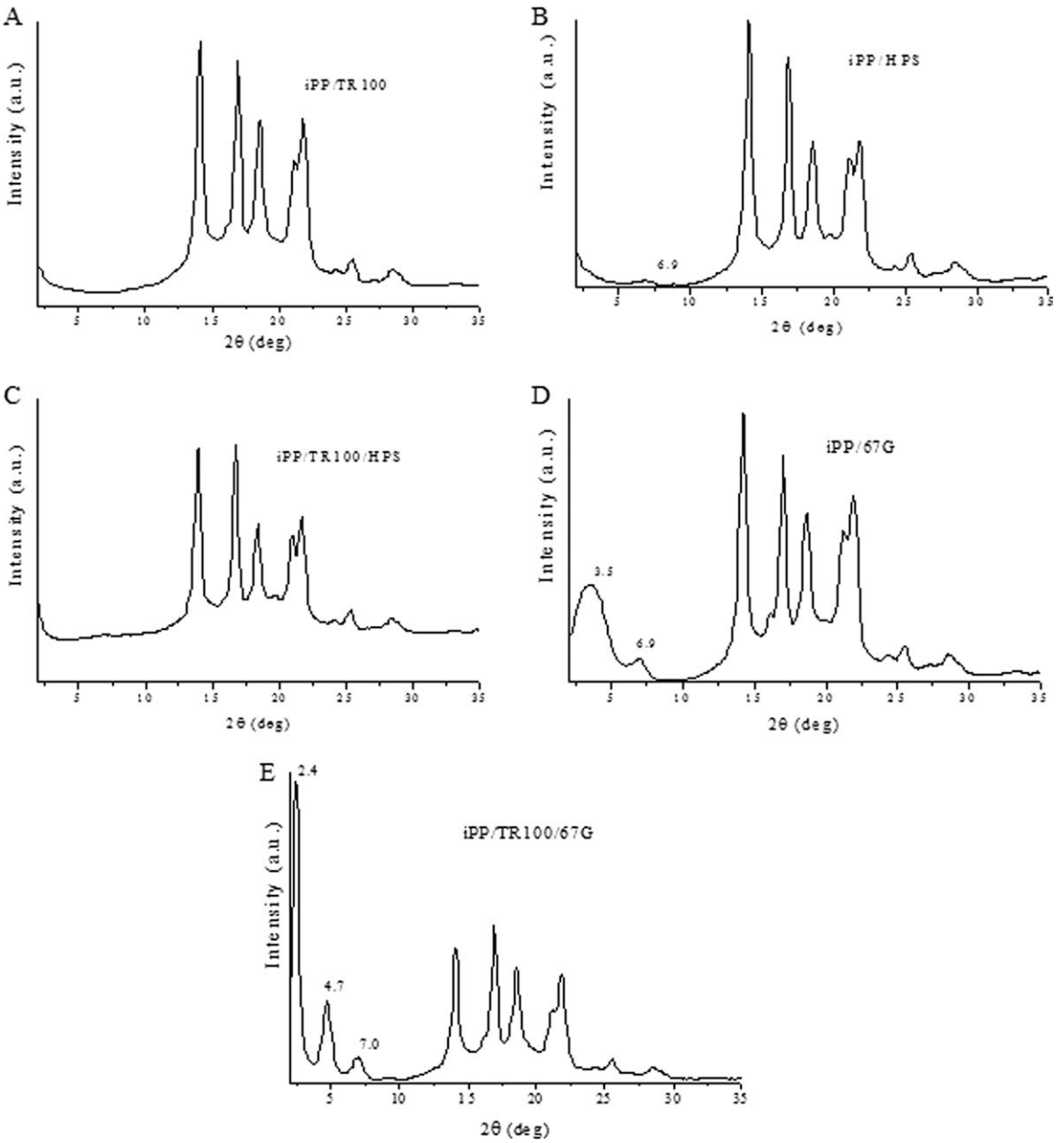

Figure 2 WAXD profiles of binary and iPP ternary systems.

montmorillonite purified and modified with a high content of quaternary ammonium salt. Interesting is the effect of the addition of the TR100 resin: both the clays result completely homogenized in the iPP matrix; in fact the micrographs of the two ternary systems [Fig. 3(D,F)] show homogeneous surfaces with no evidence of clay particles, at least for the magnification used in the investigation, 5000×. These results indicate that TR100, although does not induce any intercalation of the 67G and HPS clays in the iPP matrix [as deducible from WAXD in Fig. 2(E,C)], it certainly reduces the size of the clay domains and homogenize the clay in the iPP/TR100 matrix.

Thermo-analytical curves of iPP, iPP/TR100 and nanocomposites are reported in Figure 4(A). The thermograms present endothermic peak due to the melting of iPP crystals (T_m) and the glass transition temperature (T_g) that is pointed out by the first derivative curves shown in Figure 4(B). The T_m and T_g values are reported in Table III. It is found that the melting point of iPP decreases in all the compositions containing TR100. The decrease of T_m can be due to kinetic and thermodynamic effects.[38,39] Considering that for the three compositions with TR100 the T_g increases of 6–8° (see second column of Table III), due to the compatibility between iPP and TR100 in the amorphous phase, it can be concluded that also the thermodynamic effect, besides the kinetic effect, contributes to decrease of the T_m. The T_g and T_m values of iPP/HPS composite are similar to those

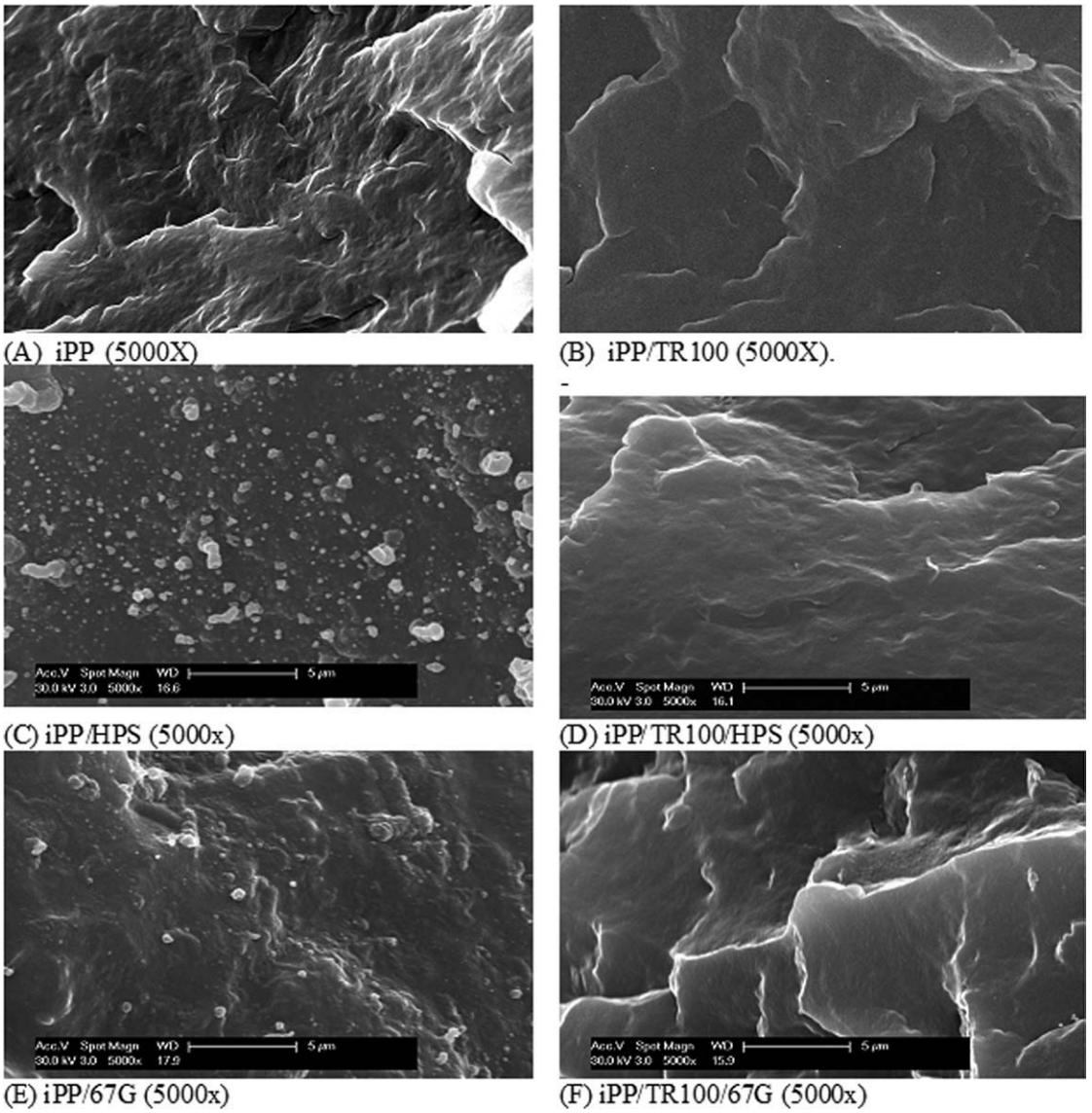

Figure 3 SEM micrographs (at 5000×) of fractured surfaces of (A) iPP; (B) iPP/TR100; (C) iPP/HPS; (D) iPP/TR100/HPS; (E) iPP/67G and (F) iPP/TR100/67G samples.

of the plain iPP, whereas for the iPP/67G the two values decrease; the reduction of T_g for iPP/67G composite is not large, but it is beyond the experimental error, indicating an influence of the iPP chain mobility following the addition of the modified clay.

Figure 5 shows the % weight loss as function of temperature in air atmosphere. The iPP and the iPP/TR100 blend have, more or less, similar thermal stability. The two clays induce different behaviors for the degradation of iPP. The iPP/HPS is the only composition that degrades before the plain iPP, whereas iPP/67G has a slight better thermal stability than iPP. This difference could be due to the different dispersion of clay in the iPP/clay composites [Fig. 3(C,E)]. It seems plausible to attribute the different behaviors to the dispersion of the clay and not to the diverse nature of them. In fact, as the TR100 resin alone does not have any effect on the thermal stability of iPP, the two ternary composites (whose SEM micrographs have revealed a good dispersion of clay in the matrix) have the highest thermal stability.

Table IV reports water vapor transmission rate and the permeability determined at 38°C and relative humidity 90%. The addition of TR100 resin decreases the permeability of the iPP based film. This effect is due to the complete compatibility in the melt between iPP and TR100 so that, after the system is cooled, the amorphous phase has a T_g higher of about 8° than that of plain iPP (Table II); so the permeability (or WVTR) decreases, although the total crystallinity is lower, 50% against 55% of

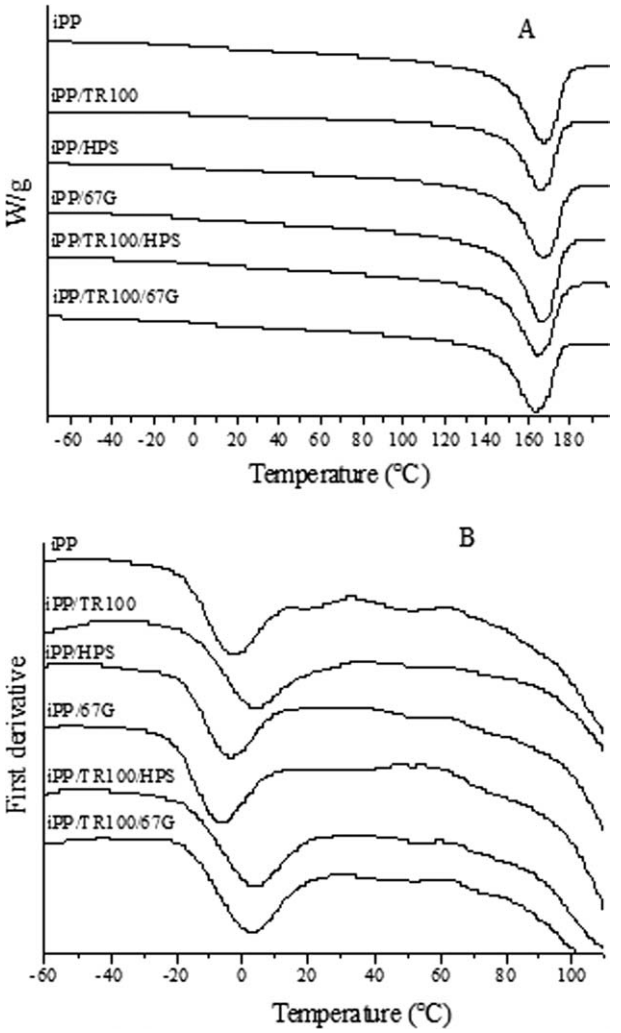

Figure 4 Thermoanalytical curves (A) and relative first-order derivatives (B).

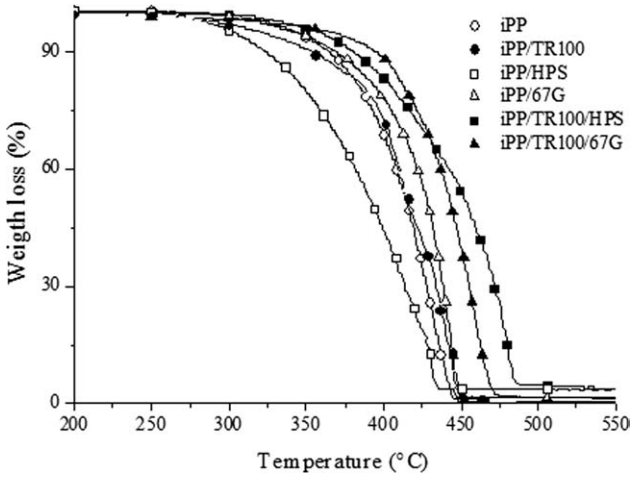

Figure 5 TGA weight loss as function of temperature.

plain iPP. Passing to the analysis of the two binary composites (i.e., iPP/HPS and iPP/67G) it is found that the presence of HPS in iPP increases the permeability to 1.3, whereas 67G clay strongly decreases the permeability to 0.35. It is worth to recall the morphologies found by SEM for these two composites [Fig. 3(C,E)]: the first system (iPP/HPS) presents many clay domains, the second one (iPP/67G) presents much less and smaller domains indicating that a quite percentage of 67G clay is homogeneously distributed in iPP matrix. The different distribution and inclusion of the two clays could be the explanation of the different values of the permeability. The addition of TR100 resin to the iPP/HPS and to iPP/67G further reduces the permeability values, not only because of the increase of T_g as discussed above for the iPP/TR100 blend, but also for the fact that the resin greatly reduces and distributes the domains of both the clays in the polymer matrix as it results from the SEM micrographs in Figure 3(D,F).

Figure 6 shows the nominal stress–strain curves of the samples tested at room temperature and Table V reports the tensile parameters averaged over 12 tests for each composition. The pristine iPP exhibits the classical behavior of a semicrystalline polymer with yielding phenomenon followed by a cold-drawing region, and finally rupture at elongation value of 840% and stress at 38 MPa. The iPP/TR100 blend presents the same tensile behavior as iPP with the only difference to have a higher value of the Young's modulus, derived by the fact that the T_g of the iPP/TR100 blend (5°C) is higher than the T_g of pristine iPP (-3°C) so that at room temperature the amorphous phase of the blend is more rigid than that of iPP. The two binary composites, iPP/HPS

TABLE III
Glass Transition (T_g) and Melting Temperature (T_m)

	T_g (°C) ±1	T_m (°C) ±0.2
iPP	−3	167.2
iPP/TR100	5	165.6
iPP/HPS	−3	167.4
iPP/67G	−6	166.8
iPP/TR100/HPS	4	164.6
iPP/TR100/67G	3	163.3

TABLE IV
WVTR and Permeability for Same Samples

Composites	WVTR [g/(24 h m^2)]	Permeability [ng/(Pa s m)] × 10^3
iPP	6.8	1.1
iPP/TR100	5.4	0.85
iPP/HPS	8.0	1.3
iPP/TR100/HPS	5.7	0.81
iPP/67G	1.6	0.35
iPP/TR100/67G	1.2	0.28

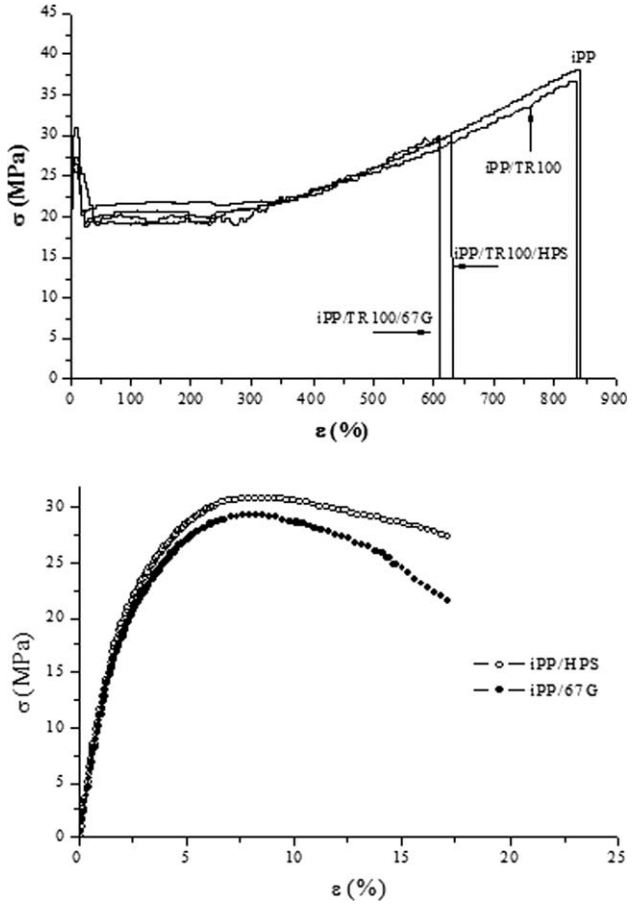

Figure 6 Nominal stress–strain curves.

and iPP/67G, show a conspicuous increase of the Young's modulus due to the clay in the matrix; but the clay is present in the polymer matrix in gross domains [as seen in SEM micrographs in Fig. 3(C,E)] that act as defects so that the rupture occurs soon after the yield point. The brittle behavior observed for the two binary composites changes when it is added TR100: the ternary systems iPP/TR100/67G and iPP/TR100/HPS show behavior similar to that of iPP but with lower rupture values, 610–630% and 30Mpa. The cold drawing and the fiber formation region are possible for the ternary system because the clays have been homogeneously distributed in the iPP matrix by the TR100 resin as shown by the SEM micrographs in Figure 3(D,F).

CONCLUSIONS

In this work, iPP/clay and iPP/TR100/clay composites were prepared by mixing in the melt directly the components. It is found that the binary iPP/HPS and iPP/67G composites are characterized by morphology presenting domains of clays in the iPP matrix; the iPP/HPS system contains many and large domains of clay clearly separated from the iPP matrix; iPP/67G contains smaller and much less clay domains indicating that a quite part of 67G clay is well distributed and embedded in iPP matrix. Both the binary systems present an increase of the Young's modulus of about 30%, compared to that of pristine iPP; the domains act as defects for the tensile drawing so that both the composites result brittle: the rupture occurs soon after the yielding point. The diverse morphologies found for the two binary composites have, instead, a different influence on the permeability to water vapor. For the iPP/HPS the values increases probably because the interface between the iPP matrix and the numerous and gross clay domains constitute a preferential and easy pathway for water molecules, whereas for the iPP/67G the permeability decreases significantly because a quite parte of 67G clay is sufficiently and homogeneously distributed and embedded in iPP matrix resulting as obstacles to the diffusions of the water molecules. The addition of Necires TR100 greatly improves the dispersion of the two clays in the iPP. The better dispersion of the clays in iPP matrix influences the tensile deformation; the ternary composites present ductile behavior with an elongation value to break point just above 600%. The better dispersion has also positive effects on the permeability values, which result to be lower than the corresponding binary composites and on the thermal degradation.

The main objective of this work was to investigate if the hydrocarbon resin Necirès TR100, containing hydroxyl and acid groups, could interact with the polar surface of the two clays Dellite HPS and Dellite 67G (this last already intercalated by quaternary ammonium salt) during the melt mixing to have further intercalation between the layers and possibly also exfoliation. The WAXD results have clearly indicated that this expectation does not occur. It is only found that Necirès TR100 is able to homogenize

TABLE V
Tensile Parameters

Sample	E (MPa)	σ_y (MPa)	ε_y (%)	σ_b (MPa)	ε_b (%)
iPP	1070 ± 90	31 ± 3	9 ± 1	38 ± 4	840 ± 70
iPP/TR100	1160 ± 60	27 ± 3	10 ± 1	37 ± 5	840 ± 55
iPP/HPS	1380 ± 130	–	–	27 ± 6	17 ± 2
iPP/TR100/HPS	1280 ± 100	26 ± 2	9 ± 1	30 ± 4	630 ± 50
iPP/67G	1330 ± 60	–	–	20 ± 3	19 ± 1
iPP/TR100/67G	1370 ± 130	26 ± 3	9 ± 1	30 ± 4	610 ± 50

and distribute the clay domains in the iPP matrix so that for the ternary nanocomposites the permeability decreases (compared to the pristine iPP and binary iPP/clay composites), the tensile elongations to break increases and the values are comparable to those of pristine iPP sample; there is also a positive effect on the thermal degradation. Finally, it is worth to mention the results found for the binary iPP/67G composite: the permeability is much lower than those of pristine iPP and iPP/HPS and this decrease is only possible if a percentage of clay is homogeneously distributed in the matrix; it is not possible to hypothesize that all the clay is distributed in the matrix because the SEM micrograph show clearly the presence of some clay domains. Moreover the finding of the peak at about 3.5°, probably the result of the merging of the 2.4 and 4.7° peak present in the plain 67G, indicate that some interaction between iPP molecules and 67G could have happened.

References

1. Usuki, A.; Kojima, Y.; Kawasumi, M.; Okada, A.; Fukushima, Y.; Kurauchi, T.; Kamigaito, O. J Mater Res 1993, 8, 1179.
2. Kojima, Y.; Usuki, A.; Kawasumi, M.; Okada, A.; Fukuscima, Y.; Kurauchi, T.; Kamigaito, O. J Mater Res 1993, 8, 1185.
3. Yano, K.; Usuki, A.; Osaka, A.; Kurauchi, T.; Kamigaito, O. J Polym Sci Part A: Polym Chem 1993, 31, 2493.
4. Vaia, R. A.; Isii, H.; Giannelis, E. P. Chem Mater 1993, 5, 1664.
5. Lan, T.Pinnavaia, T. Chem Mater 1994, 6, 2216.
6. Biasci, L.; Aglietto, M.; Ruggeri, G.; Ciardelli, F. Polymer 1994, 35, 3296.
7. Richard, A. V.; Jandt, K. D.; Edward, J. K.; Giannelis, E. P. Macromolecules 1995, 28, 8080.
8. Messersmith, P. B.; Giannelis, E. P. J Polym Sci Part A: Polym Chem 1995, 33, 1047.
9. Kato, M.; Usuki, A.; Okada, A. J Appl Polym Sci 1997, 66, 1781.
10. Hasegawa, N.; Kawasumi, M.; Kato, M.; Usuki, A.; Okada, A. J Appl Polym Sci 1998, 67, 87.
11. Giannelis, E. P. Appl Organomet Chem 1998, 12, 675.
12. Gilman, J. W.; Jackson, C. L.; Morgan, A. B.; Harris, R.; Manias, E.; Giannelis, E. P.; Wuthenow, M.; Hilton, D.; Phillips, S. H. Chem Mater 2000, 12, 1866.
13. Hasegawa, N.; Okamoto, H.; Kato, M.; Usuki, A. J Appl Polym Sci 2000, 78, 1918.
14. Biswas, M.Sinha Ray, S. Adv Polym Sci 2001, 155, 167.
15. Xu, R.; Manias, E.; Snyder, A. J.; Runt, J. Macromolecules 2001, 34, 337.
16. Tjong, S. C.; Meng, Y. Z.; Xu, Y. J Appl Polym Sci 2002, 86, 2330.
17. Sinha Ray, S.; Yamada, K.; Okamoto, M.; Ueda, K. Nano Lett 2002, 2, 1093.
18. Sinha Ray, S.; Yamada, K.; Okamoto, M.; Ueda, K. Macromol Mater Eng 2003, 288, 203.
19. Sinha Ray, S.Okamoto, M. Prog Polym Sci 2003, 28, 1539.
20. López-Quintanilla, M.; Sánchez-Valdés, S.; Ramos De Valle, L. F.; Medellín-Rodríguez, F. J. J Appl Polym Sci 2006, 100, 4748.
21. Chen, M.; Wan, C.; Shou, W.; Zhang, Y.; Zhang, J. J Appl Polym Sci 2008, 107, 1718.
22. Lee, H.Kim, D. S. J Appl Polym Sci 2009, 111, 2769.
23. Ku, K. H.Kim, S. C. J Appl Polym Sci 2009, 113, 1539.
24. Kandola, B. K.; Smart, G.; Horrocks, A. R.; Joseph, P.; Zhang, S.; Hull, T. R.; Ebdon, J.; Hunt, B.; Cook, A. J Appl Polym Sci 2008, 108, 816.
25. Song, P.; Tong, L.; Fang, Z. J Appl Polym Sci 2008, 110, 616.
26. Tarapow, J. A.; Bernal, C. R.; Alvarez, V. A. J Appl Polym Sci 2009, 111, 768.
27. Meng, X.; Wang, Z.; Du, X.; Wang, Y.; Tang, T. J Appl Polym Sci 2009, 113, 678.
28. Shariatpahahi, H.; Sarabi, F.; Mirali, M.; Hemmati, M.; Mahdavi, F. J Appl Polym Sci 2009, 113, 922.
29. Ahmad Ramazzani, S. A.; Tavakolzadeh, F.; Baniasadi, H. J Appl Polym Sci 2010, 115, 308.
30. Wang, W. Y.; Wang, G. Q.; Zeng, X. F.; Chen, J. F. J Appl Polym Sci 2010, 115, 911.
31. Du, X.; Zhang, Z.; Yu, H.; Wan, D.; Xing, H.; Tang, T. J Appl Polym Sci 2010, 115, 1105.
32. Karian, H. G. Handbook of Polypropylene and Polypropylene Composites; Marcel Dekker, Inc.: New York-Basel, 1999.
33. Freedonia Group. Polypropylene to 2004-Market Size, Market Share, Demand Forecast and Sales, Industry Study n.1305; Freedonia Group: Cleveland, Ohio, 2000.
34. Usuki, A.; Kato, M.; Okada, A.; Kurauchi, T. J Appl Polym Sci 1997, 63, 137.
35. Cimmino, S.; Silvestre, C.; Duraccio, D. unpublished.
36. Bruckner, S.; Mille, S. V.; Petraccone, V.; Pirozzi, B. Prog Polym Sci 1991, 16, 361.
37. Silvestre, C.; Cimmino, S.; Di Pace, E. In Handbook of Polyolefins, 2nd ed. ; Vasile, C., Ed.; Marcell Dekker: New York-Basel, 2000; Chapter 7.
38. Nishi, T.; Wang, T. T. Macromolecules 1975, 8, 909.
39. Kwei, T. K.Frisch, H. L. Macromolecules 1978, 11, 1267.